Progress In Electromagnetics Research, Vol. 134, 63–78, 2013

REDUCTION OF INTERNAL REFLECTIONS IN INTEGRATED LENS ANTENNAS FOR BEAM-STEERING

Aki Karttunen[1, *], Juha Ala-Laurinaho[1], Ronan Sauleau[2], and Antti V. Räisänen[1]

[1]SMARAD/MilliLab, Department of Radio Science and Engineering, Aalto University School of Electrical Engineering, P. O. Box 13000, AALTO FI-00076, Finland

[2]Institute of Electronics and Telecommunications of Rennes (IETR), UMR CNRS 6164, University of Rennes 1, Rennes 35042, France

Abstract—The conventional integrated lens antennas (ILAs) for beam steering suffer from internal reflections that deteriorate the scanning properties. The internal reflections are known to affect side lobes, cross-polarisation level, input impedance of the feed, and mutual coupling. In this paper, ILAs are designed to exhibit very low reflection loss, i.e., to minimize the internal reflections. Wide ranges of realistic relative permittivities of the lens and of the feed element directivities are considered. It is shown that with any permittivity and with any feed directivity it is possible to design the lens shape in such a way that the reflection loss is low, for moderate beam-steering angles, without resorting to a complicated matching layer. The gain, directivity, beam-width, and the resulting distance between the feed elements are compared for all the designed lenses.

1. INTRODUCTION

Integrated lens antenna (ILA) can be used as a narrow-beam high-directivity beam-steering antenna. Such antennas can find use, e.g., in automotive radar at 77–81 GHz with high angular resolution [1] or telecommunications for high data rate links in E-band (71–86 GHz) [2–4]. With ILA, electrical beam-steering is done by switching between the feed elements of a feed array [3–5]. The lens collimates the radiation of the relatively low-directivity feed array antenna element, and the main beam direction is relative to the active element's distance to the

Received 22 October 2012, Accepted 15 November 2012, Scheduled 21 November 2012

* Corresponding author: Aki Karttunen (aki.karttunen@aalto.fi).

rotational symmetry axis of the lens. The beam-steering principle is illustrated in Fig. 1.

The conventional types of ILAs are the extended hemispherical [3–8] and the elliptical lenses [4, 8–13]. Diffraction-limited patterns are attained with an elliptical lens that has an eccentricity of $e = (\varepsilon_r)^{-1/2}$, and extension length $L = e \cdot a$, where ε_r is the relative permittivity of the lens material and a the semimajor axis of the ellipse. With relatively small beam-steering angles up to about 15°–25°, the elliptical lens is better, but for larger angles the extended hemispherical lens is more appropriate [4, 9].

In this study, $20\lambda_0$-diameter ILAs are designed for approximately maximum of ±15° beam-steering range. Larger lenses would be unpractical, because of their large size and heavy weight, and because they are lossy even with relatively low loss materials. The beam-steering angular range is limited because of the relatively narrow beam and limited number of beams due to increasing switching network loss. For beam-steering with wider beam, i.e., smaller antenna, or wider beam-steering range, phased array could be considered [14].

Elliptical ILAs with a wide range of permittivities (ε_r = 2.5, 4, and 12) with a wide range of feed element directivities (D_{feed} = 4.5 dB, 7.8 dB, and 11.5 dB) are designed. The lenses are shaped in such a way that the reflection loss is low for all ε_r & D_{feed} combinations for the whole beam-steering range. The reflection loss is defined as

$$L_{refl} = 10 \cdot \log_{10}(P_{tot}/(P_{tot} - P_{refl})), \tag{1}$$

where P_{refl} is the total reflected power and P_{tot} the total power radiated into the lens. In the case of conventional ILAs, the internal reflections are known to affect the radiation pattern [4, 6, 10–12], input impedance of the feed [4, 11], and the mutual coupling [13].

The ILA design principle and method to reduce the internal reflections are described in Section 2, and the simulation results are presented in Section 3. Discussion and conclusions are given in Sections 4 and 5, respectively.

2. ILA FOR BEAM STEERING

A conventional elliptical ILA has an eccentricity of $e = (\varepsilon_r)^{-1/2}$. The feed array is in direct contact with the planar bottom of the lens (Fig. 1). The part of the lens that is between the planar lens bottom and the elliptical part is called extension. Typically a cylindrical extension is used [3–5, 7, 9–13]. The extension length L of an elliptical ILA is $L = e \cdot a$, where ε_r is the relative permittivity of the lens material and a the semimajor axis of the ellipse. The eccentricity of an ellipse

is defined as

$$e = \sqrt{1 - (b/a)^2}, \tag{2}$$

where b is the semiminor axis of the ellipse. In conventional elliptical ILAs, the lens radius R is the same as the semiminor axis of the ellipse.

The simulation method used in this study is a commonly used ray-tracing simulation, as e.g., in [7]. The first step is to trace the rays from the feed to the lens surface and to calculate the field outside the lens. Ray-tracing uses Snell's law on the lens surface and the power conservation law inside elementary ray tubes. Secondly, the equivalent electric and magnetic surface currents are calculated on the lens surface, and then the far-field is computed from the equivalent currents. Ray-illustrations of conventional elliptical lenses are shown

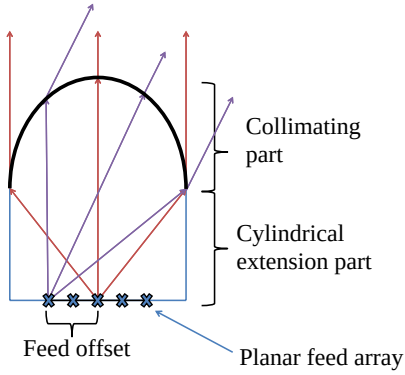

Figure 1. An illustration of the beam-steering principle. Feed offset is defined as the feed element distance from the rotational symmetry axis of the lens. These rays are selected for illustrative purposes only.

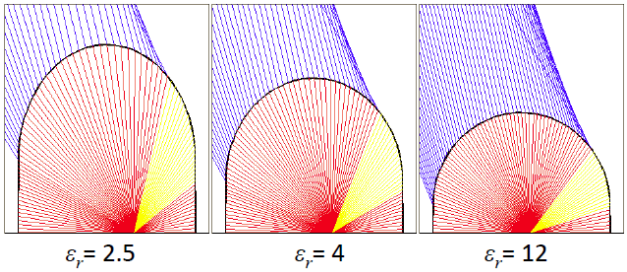

Figure 2. Ray illustrations with the maximum offset; Conventional elliptical lenses with $\varepsilon_r = 2.5$, $\varepsilon_r = 4$, and $\varepsilon_r = 12$. Yellow rays are totally reflected.

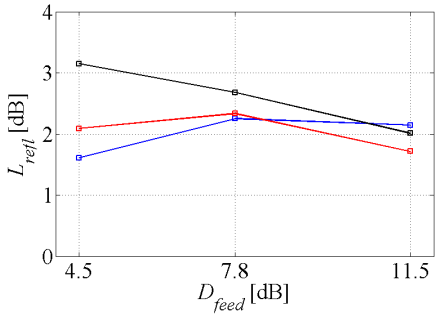

Figure 3. Reflection loss with the maximum offset; Conventional elliptical lenses with $\varepsilon_r = 2.5$ (blue), $\varepsilon_r = 4$ (red), and $\varepsilon_r = 12$ (black).

in Fig. 2.

All the lenses designed in this work are $20\lambda_0$-diameter ($R = 10\lambda_0$) elliptical lenses with $e = (\varepsilon_r)^{-1/2}$. Lens permittivities $\varepsilon_r = 2.5$, $\varepsilon_r = 4$, and $\varepsilon_r = 12$ are compared. These permittivity values give good approximations of realistic low, medium, and high permittivity materials. For simplicity, the lens materials are assumed to be lossless.

Beam-steering range of about $\pm 15^\circ$ is targeted and the consequent maximum feed offset $x_{\max}$ is determined for all the lenses using Snell's law. Good approximation of the beam direction can be obtained by tracing a ray through the top of the lens (Fig. 4(c)). The maximum feed offset gives an approximate beam direction of 13° ($\pm 13^\circ$ + half-power beam-width $\approx \pm 15^\circ$).

The feed radiation pattern is considered to be a point source with amplitude pattern

$$|\overline{E}(\phi, \theta)| = \cos^N(\theta), \quad 0 \leq \theta \leq 90^\circ, \quad 0 \leq \phi \leq 360^\circ, \tag{3}$$

at the main polarization of Ludwig's second definition of polarization [15]. The directivity of the feed element is varied with the parameter N. Feed element directivities $D_{\text{feed}} = 4.5\,\text{dB}$ ($N = 0.2$), $7.8\,\text{dB}$ ($N = 1$), and $11.5\,\text{dB}$ ($N = 3$) are used. These values give good approximations of realistic low, medium, and high feed element directivities. In total nine ε_r & D_{feed} combinations are considered.

The simulated reflection loss with the conventional ILAs is shown in Fig. 3. Typically with ILA the reflection loss increase as a function of the feed offset [4, 6, 7, 12]. The reflection loss in Fig. 3 is quite high for all ε_r & D_{feed} combinations. This is largely due to total reflections which are shown in yellow in Fig. 2.

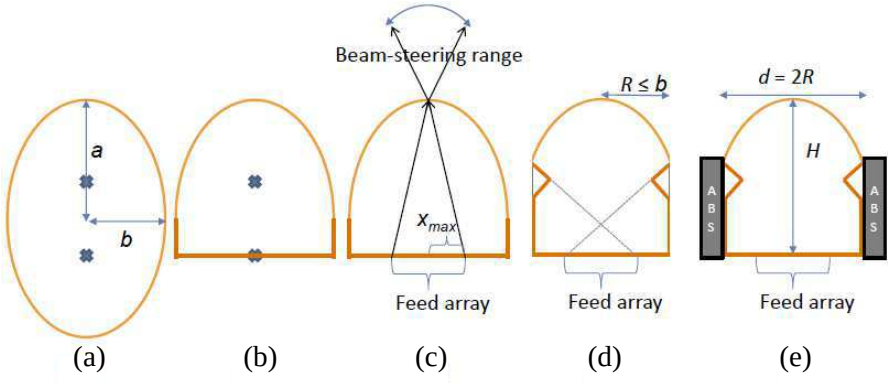

Figure 4. (a)–(c) Illustration of conventional lens and (d)–(e) proposed method for reduction of internal reflections. (a) Ellipse with eccentricity $(\varepsilon_r)^{-1/2}$. (b)–(c) Center of a planar feed array is placed to the more distant foci of the ellipse. (d) Only a radius of $R \leq b$ of the ellipse is used and the rest of the lens is shaped to avoid total reflections. (e) Absorber around the extension to capture the spill over field.

2.1. Reduction of Internal Reflections

Here we suggest to modify the lens shape of a conventional elliptical ILA in order to reduce the internal reflections. In [6], the authors presented a shaped low permittivity extended hemispherical lens design that has very low reflection loss. In [8], absorbers are used around a shaped extension of a low permittivity elliptical lens to reduce high side-lobe levels caused by spillover fields, i.e., field exiting from the extension part of the lens. The shaping used in [6, 8] is not directly applicable to all lens permittivities with the elliptical shape, and therefore, this method is modified and generalized in this paper.

The lens design method to reduce the internal reflections is illustrated in Fig. 4, and ray-illustrations of the designed lenses are shown in Figs. 5–7. The lens shape is designed in three steps:

1) Conventional elliptical ILA (Figs. 4(a)–(c)).
2) Only a radius of $R \leq b$ of the ellipse is used. The ratio b/R together with ε_r controls the lens height-to-diameter ratio H/d, shown in Fig. 8(a). With conventional ILA this ratio is solely determined by ε_r. The ratio b/R also affects the maximum feed offset $x_{\max}$ needed for the same beam-steering range. The maximum feed offsets are shown in Fig. 8(b).

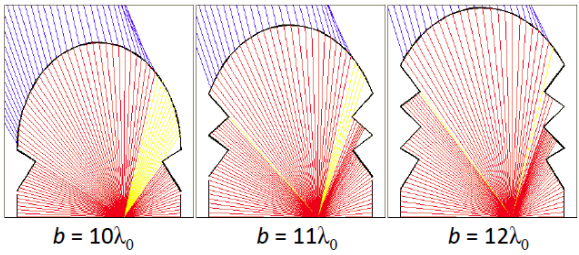

Figure 5. Ray illustrations with the maximum offset, with $\varepsilon_r = 2.5$, and with different original ellipse minor axis b, and radius $R = 10\lambda_0$. Yellow rays are totally reflected.

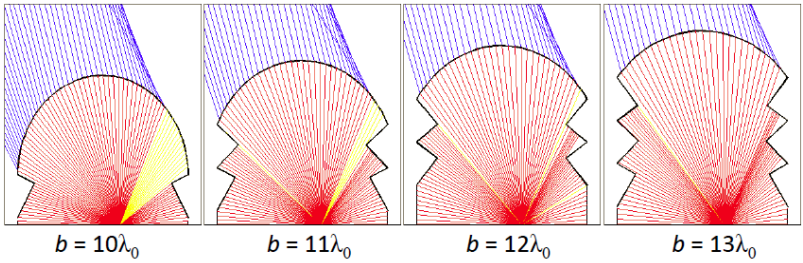

Figure 6. Same as Fig. 5, with $\varepsilon_r = 4$.

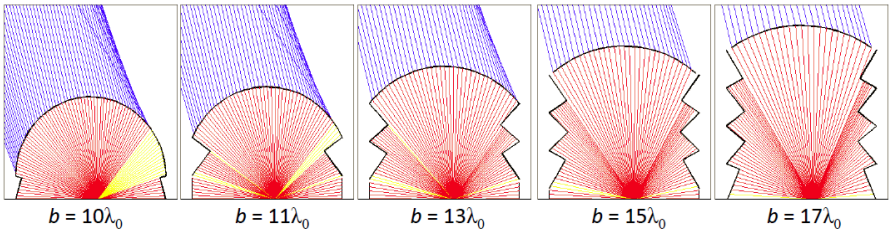

Figure 7. Same as Fig. 5, with $\varepsilon_r = 12$.

3) The shape of the lens surface between the planar bottom and the elliptical part is designed for minimal reflections, i.e., minimized angle between surface normal and ray direction. In this study, $5\lambda_0$-wide circumferential grooves, in the lens height direction, are made to the lens. The angle of the grooves is made to point towards the maximum feed offset, as illustrated in Fig. 4(d) and in ray illustrations Figs. 5–7. The advantages of these grooves are reduced lens volume and simple shape with only conical and

cylindrical surfaces in the extension. Similar shape has been used successfully (with low permittivity ILAs) in [6, 8]. The grooved extension shape, used in this study, is only one example of usable shapes. Any extension shape that minimizes, or at least reduces, the internal reflections is a useful extension shape.

Conventionally, a quarter-wave matching-layer is used to reduce the internal reflections, e.g., [9–11]. However, a matching layer does not reduce the total reflections as the critical angle for total reflections does not change. Instead, with a shaped lens the total reflections can be reduced (Figs. 5–7). A matching layer for the doubly curved elliptical surface is difficult to manufacture. On the other hand, the extension has only conical and cylindrical surfaces. The matching layer on the extension is considered to be much easier to manufacture and it is even allowed to be discontinuous as the continuity of reflected or spillover fields is irrelevant. In this work, a quarter-wave matching-layer is considered, if needed, for the shaped extension.

Spillover loss, i.e., fields coming out from the extension, can increase side-lobe levels, e.g., [4, 8]. Therefore, there is no reason to allow the spillover field to leak to the far-field. In case of ILA with large extension, the use of the absorber can increase the directivity by several decibels, e.g., in [8] a 3.1 dB directivity improvement is reported due to lower side-lobes. Absorber is placed around the extension (Fig. 4(e)) in order to make sure that the spillover does not affect the far-field.

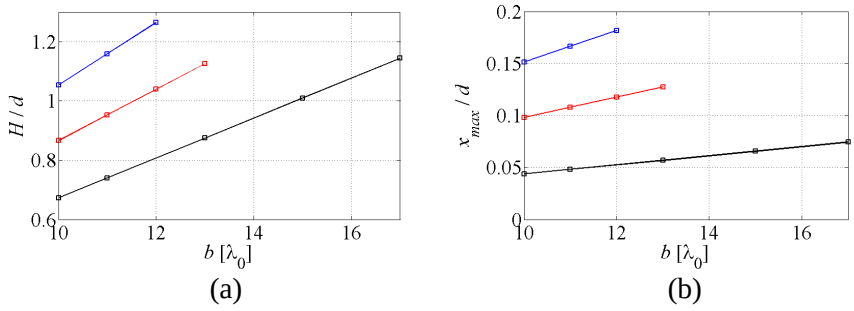

Figure 8. (a) Lens height compared to diameter (H/d), and (b) the maximum offset compared to diameter ($x_{\max}/d$); With different original ellipse minor axis b, and radius $R = 10\lambda_0$. $\varepsilon_r = 2.5$ (blue), $\varepsilon_r = 4$ (red), and $\varepsilon_r = 12$ (black).

3. RESULTS

The simulation results are organised as follows: the reflection loss is presented and discussed in Subsection 3.1, the simulated gain, and other far-field parameters in Subsection 3.2, and the resulting distance between the feed elements in Subsection 3.3. These results are generalized in Section 4.

3.1. Reflection Loss

The simulated reflection loss with the maximum offset $x_{\max}$, that results in a main beam at 13°, is presented in Fig. 9. Reflection loss with a quarter-wave matching-layer in the extension is also presented. Lenses with $R = b$ have high reflection loss, nearly the same as with the conventional elliptical ILAs in Fig. 3, showing that simply shaping the extension of an elliptical lens is not sufficient.

Low reflection loss ($L_{refl} < 1\,\mathrm{dB}$) is easily achieved with low and medium lens permittivities, i.e., with $\varepsilon_r = 2.5$ or $\varepsilon_r = 4$, when

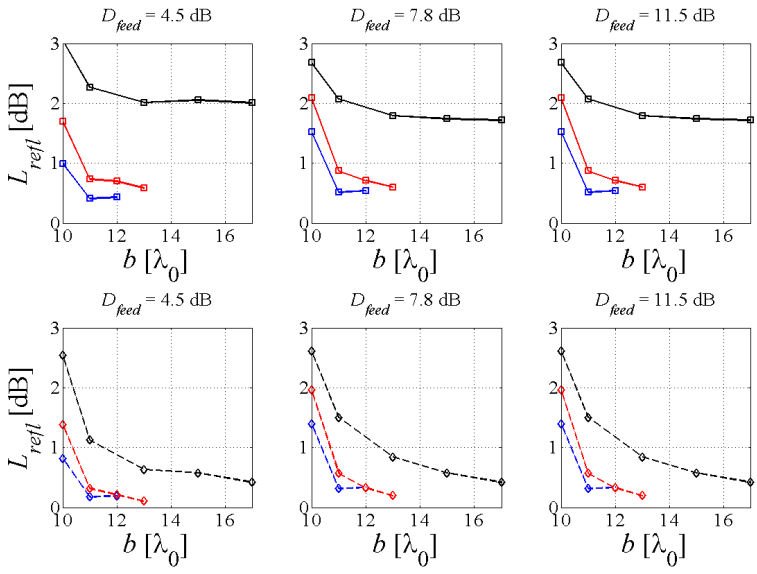

Figure 9. Simulated reflection loss with the maximum offset. $\varepsilon_r = 2.5$ (blue), $\varepsilon_r = 4$ (red), and $\varepsilon_r = 12$ (black) with different original ellipse minor axis b, and radius $R = 10\lambda_0$; No matching layer (□) and a quarter wave matching layer in the extension (◊).

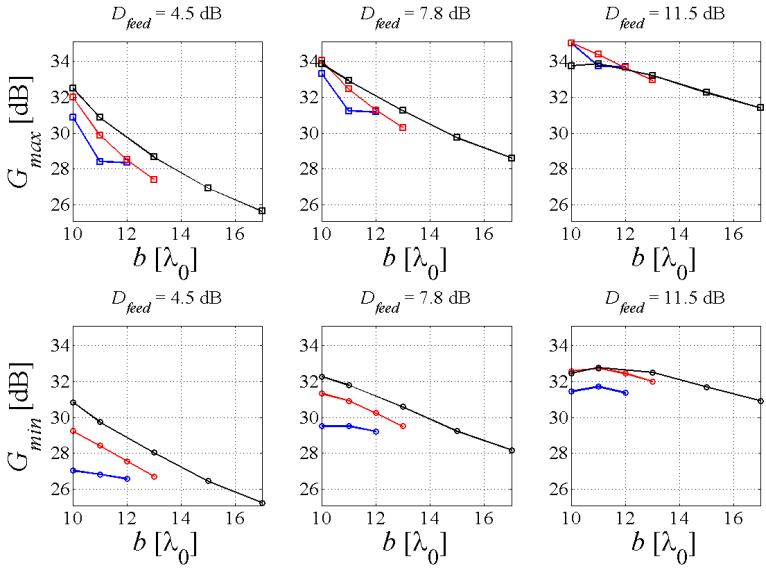

Figure 10. Simulated maximum gain (without feed offset) and minimum gain (with maximum offset). $\varepsilon_r = 2.5$ (blue), $\varepsilon_r = 4$ (red), and $\varepsilon_r = 12$ (black) with different original ellipse minor axis b, and radius $R = 10\lambda_0$.

$b \geqslant 1.1 \cdot R$, with any D_{feed}, and without any matching layer. High permittivity lens requires a matching layer and larger b/R ($\varepsilon_r = 12$: $L_{refl} < 1\,\text{dB}$ with $b \geqslant 1.3 \cdot R$, with any D_{feed}, and matching layer to the extension). Even reflection loss lower than 0.5 dB is possible with any ε_r & D_{feed} combination using matching layer, although it requires very large b/R with high permittivity lenses. The maximum presented b/R for each ε_r is selected such that $L_{refl} < 0.5\,\text{dB}$ is possible at least with the matching layer to the extension. With larger b/R there is no significant improvement in L_{refl} and the gain decreases (see Fig. 10).

3.2. Far-field Results

Only the rays exiting from the elliptical part of the lens without reflection are considered for the far-field results. This is sufficient as the reflection loss is low and absorber is placed around the extension to capture the spillover fields. Gain, directivity, and half-power beamwidth (HPBW) are presented in Figs. 10–12 for all ε_r, b, and D_{feed} without feed offset and with the maximum feed offset. Simulation without feed offset gives the maximum gain and directivity and the

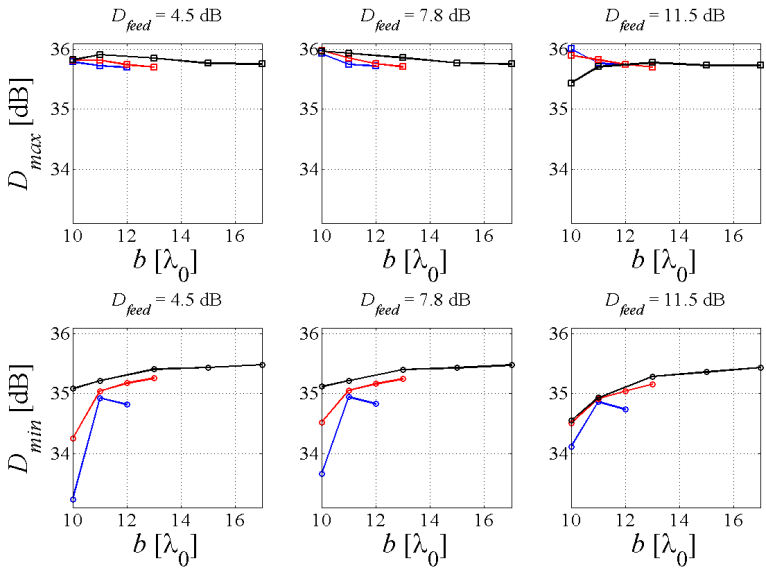

Figure 11. Simulated maximum directivity (without feed offset) and minimum directivity (with maximum offset). $\varepsilon_r = 2.5$ (blue), $\varepsilon_r = 4$ (red), and $\varepsilon_r = 12$ (black) with different original ellipse minor axis b, and radius $R = 10\lambda_0$.

minimum beam width. Simulation with maximum offset gives the minimum gain and directivity and maximum beam width.

One of the most important parameters of a beam-steering antenna is the minimum gain for the desired beam-steering angular range. Because the losses increase and the phase errors in the lens aperture increase as a function of the feed offset the minimum gain is achieved with the maximum offset. As can be seen from Fig. 10, minimum gain is proportional to ε_r and D_{feed} and inversely proportional to b/R. As an exception, the minimum gain is nearly constant with high D_{feed} and moderate b/R. The differences in the simulated gains are mostly due to different total losses in the lens. The differences in directivities are mostly due to differences in beam widths, see Figs. 11–12.

3.3. Distance between Feed Elements

The reduction of reflection loss includes optimization of b/R, which in turn affects the feed element separation. The distance between the neighbouring feed elements can be calculated from the desired minimum beam-overlap level, minimum beam-width, and from the

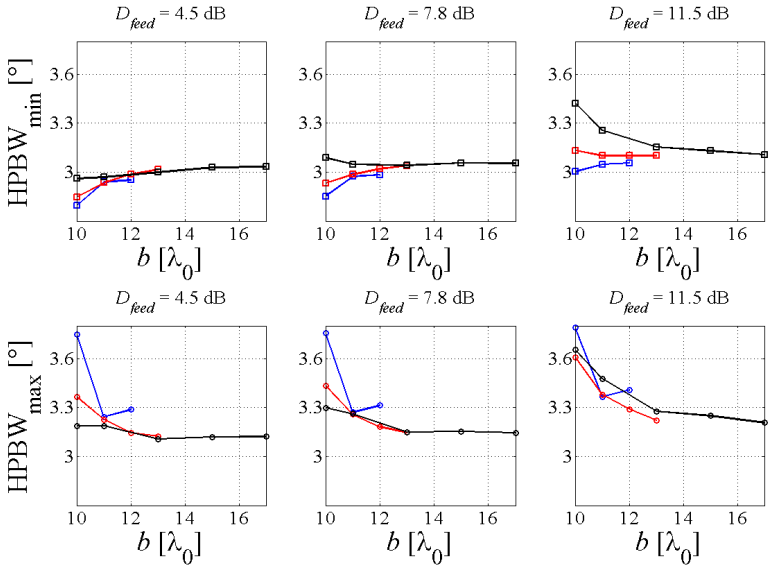

Figure 12. Simulated minimum half-power beam-width (without feed offset) and maximum half-power beam-width (with maximum offset). $\varepsilon_r = 2.5$ (blue), $\varepsilon_r = 4$ (red), and $\varepsilon_r = 12$ (black) with different original ellipse minor axis b, and radius $R = 10\lambda_0$.

beam direction as a function of the feed offset. It is considered that a continuous coverage requires that the adjacent beams overlap at 3 dB level below maximum. Hexagonal arrangement of the feeds is considered as it gives the maximum scan coverage with minimum number of feed elements [12]. The distance between the feed elements is an important parameter for the feed array design and affects, e.g., mutual coupling between the elements.

The distance between feed elements can be also approximated from the lens dimensions by tracing rays through the top of the lens. The ratio between the feed element distance for the 3 dB beam overlap $\Delta_{3\,\mathrm{dB}}$, and the wavelength inside the lens material λ_{lens}, is given as

$$\frac{\Delta_{3\,\mathrm{dB}}}{\lambda_{\mathrm{lens}}} \approx \frac{\sqrt{3}}{2}\frac{H}{d}, \tag{4}$$

where the constant $\sqrt{3}/2$ comes from the hexagonal arrangement of the feeds [12], and H/d is the lens height-to-diameter ratio in Fig. 8. In (4) it is assumed that $\Delta_{3\,\mathrm{dB}} \ll H$ and HPBW $\approx \lambda_0/d$. Similar equation can be also derived for a parabolic reflector $\Delta_{3\,\mathrm{dB}}/\lambda_0 \approx (\sqrt{3}/2)(F/d)$, where F/d is the focal length to diameter ratio. In Fig. 13, the distance

between the feed elements is compared to the wavelength inside the lens material. The $\Delta_{3\,\mathrm{dB}}$ in Fig. 13 is calculated from the simulation results, and therefore, it follows (4) only approximately.

In order to take into account the differences in the feed element directivities, the distances between the feed elements are compared to the feed element effective aperture areas:

$$A_e = \frac{G_{\mathrm{feed}}\lambda_{\mathrm{lens}}^2}{4\pi}, \tag{5}$$

where G_{feed} is the gain of the feed element. Since $G_{\mathrm{feed}} \leq D_{\mathrm{feed}}$, the maximum diameter of the feed element effective area is defined as

$$d_{e\,\max} = \frac{\lambda_{\mathrm{lens}}}{\pi}\sqrt{D_{\mathrm{feed}}}. \tag{6}$$

In Fig. 13, the distance between the feed elements is compared to the maximum diameter of the feed element effective area. Small $\Delta_{3\,\mathrm{dB}}/d_{e\,\max}$ implies possible difficulties for designing the feed array with high directivity feed elements ($D_{\mathrm{feed}} = 11.5\,\mathrm{dB}$).

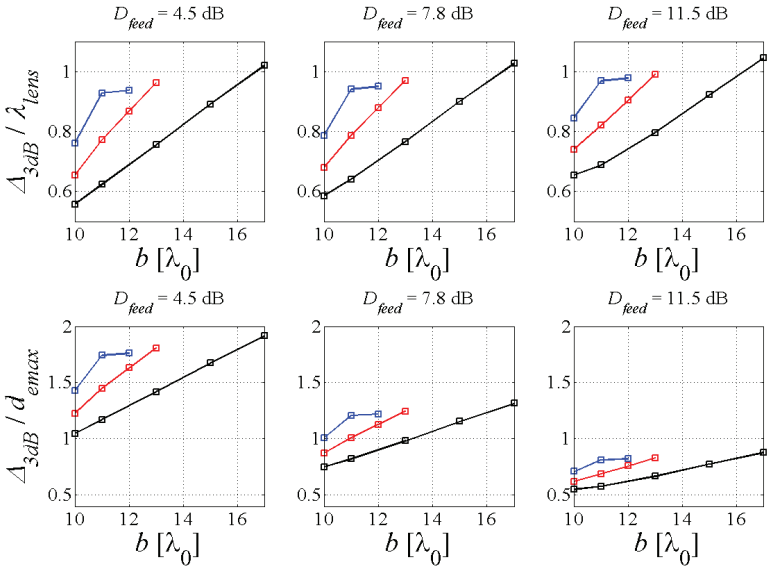

Figure 13. Distance between the feed elements $\Delta_{3\,\mathrm{dB}}$ compared to the wavelength inside the lens material λ_{lens} and compared to the maximum diameter of a feed element effective aperture area $d_{e\,\max}$. $\varepsilon_r = 2.5$ (blue), $\varepsilon_r = 4$ (red), and $\varepsilon_r = 12$ (black) with different original ellipse minor axis b, and radius $R = 10\lambda_0$.

4. DISCUSSION

The simulation results provided in this work are given for one frequency, one lens diameter, etc.. These results are generalized in the following.

Bandwidth — The bandwidth needs to be taken into account in the beam-steering ILA design. Assuming that the presented results are given for the minimum frequency $f_{\min}$, the effects of $f_{\max}/f_{\min}$ can be listed as follows. As $\lambda \propto 1/f$, it can be assumed that $D \propto f^2$ and HPBW $\propto 1/f$. The minimum gain is given at $f_{\min}$ with maximum offset ($G_{\min}$ in Fig. 10), and the maximum gain at $f_{\max}$ without offset ($\approx (f_{\max}/f_{\min})^2 \cdot G_{\max}$ in Fig. 10). The main effect of bandwidth is on the distance between the feed elements, as $\Delta_{3\,\mathrm{dB}} \propto 1/f$. The minimum beam overlap is determined at the minimum beam-width, i.e., at $f_{\max}$ without offset. In Fig. 13, $\Delta_{3\,\mathrm{dB}}/\lambda_{\mathrm{lens}}$-values do not change, but the wavelength is the maximum wavelength at $f_{\max}$. However, the $\Delta_{3\,\mathrm{dB}}/d_{e\,\min} \propto 1/f$, assuming that $D_{\mathrm{feed}} \propto G_{\mathrm{feed}} \propto f^2$. When increasing the bandwidth, $G_{\max}/G_{\min}$ increases and the feed elements have to be closer to each other.

Lens diameter — The lens diameter affects the gain and the beam-width. For example, let us assume that ε_r and H/d are kept the same, and the same feed array is used (i.e., the same maximum feed offset and the same distance between the feeds). The beam-steering range decreases as a function of the lens diameter because the maximum offset compared to the lens diameter decreases. The minimum beam overlap does not change because both the beam-width and the beam direction angles decrease. $G_{\max}/G_{\min}$ decreases because of the smaller beam-steering range resulting in smaller scan loss.

Cross-polarization — The simple feed radiation pattern (Eq. (3)) does not include cross-polarization. The simulated cross-polarization with all of the lenses in this study is below $-35\,\mathrm{dB}$ and decreasing as a function of b/R (not shown for brevity). Typically the cross-polarization of an ILA is mostly determined by the cross-polarization of the feed element and also by the reflected fields. Only with very low cross-polarization feed elements the depolarization by the lens affects the cross-polarization level of an ILA with low reflection loss.

Dielectric loss — Lossless lens materials are used in this study as approximation of good low loss materials. The dielectric loss in the lens decrease the gain. It is proportional to the loss tangent of the material and to the lens height. It also affects slightly the aperture illumination, and thus the radiation pattern, but these effects are minor.

Accuracy — The reflected fields are not calculated in the ray-tracing simulations in this study. They could be calculated with

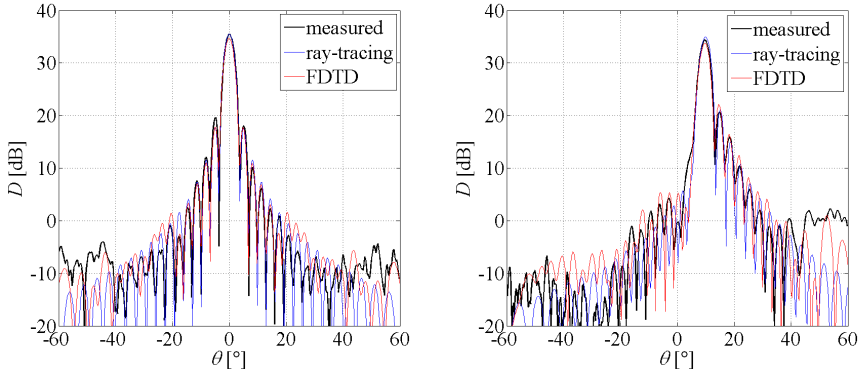

Figure 14. H-plane directivity patterns of an elliptical Rexolite ILA ($\varepsilon_r = 2.53$, $\tan\delta = 0.0013$, $b/R \approx 1.07$, $d \approx 19.3\lambda_0$) with an open-ended wave-guide as a feed ($D_{\text{feed}} \approx 8.5\,\text{dB}$). Comparison between the measured, ray-tracing simulation, and FDTD simulation results (a) without feed offset and (b) with feed offset of about $0.11 \cdot d$ resulting in main-beam maximum direction of about 10°.

ray tracing, as e.g., in [10, 12]. With a lens with low reflection loss, designed as presented in this paper, it is not necessary to calculate the reflected fields as the simple ray-tracing simulation predicts the radiation pattern very accurately, as shown in Fig. 14. In Fig. 14, measured and simulated patterns of elliptical Rexolite ILA ($\varepsilon_r = 2.53$, $\tan\delta = 0.0013$, $b/R \approx 1.07$, $d \approx 19.3\lambda_0$) with an open-ended wave-guide as a feed ($D_{\text{feed}} \approx 8.5\,\text{dB}$) are compared. The simulated reflection loss is $L_{refl} \leq 0.5\,\text{dB}$ with the presented feed offsets. The lens used is the same as in [8]. The ray-tracing and measured patterns are also compared to radiation patterns simulated with FDTD. Ray tracing predicts the radiation patterns accurately and the accuracy is as good as with the full-wave FDTD simulation.

5. CONCLUSION

Elliptical integrated lens antennas (ILAs) with low reflection loss are designed. The reduction of internal reflections is based on the selection of the original ellipse radius larger than the final lens radius and designing the shape of the extension for minimal reflections. It is shown that it is possible to design an integrated lens antenna for beam-steering with low reflection loss with any lens permittivity and with any feed element directivity.

Simulation results are given for $20\lambda_0$-diameter ILAs designed for approximately $\pm 15^\circ$ beam-steering range. The effects of the antenna parameters on the reflection loss, lens shape, gain, directivity, beam width, and on the distance between the feed elements are presented and analysed in detail.

ACKNOWLEDGMENT

This work was supported in part by the Academy of Finland through the Centre of Excellence program (SMARAD), and Tekes through BRAWE and BEAMS projects. The authors would like to thank Dr. N. T. Nguyen for his help with the FDTD simulations.

REFERENCES

1. Rasshofer, R. R. and K. Naab, "77 GHz long range radar systems status, ongoing developments and future challenges," *Proc. 2nd Eur. Radar Conf.*, 161–164, Paris, France, 2005.
2. ETSI-Standard, ETSI EN 302 217-4-2 v1.4.1, "Fixed radio systems; Characteristics and requirements for point-to-point equipment and antennas; Part 4–2: Antennas," 36, Aug. 2008.
3. Ala-Laurinaho, J., A. Karttunen, J. Säily, A. Lamminen, R. Sauleau, and A. V. Räisänen, "Mm-wave lens antenna with an integrated LTCC feed array for beam steering," *Proc. 4th Eur. Conf. Antennas Propag.*, C09P1-2/1841151, Barcelona, Spain, Apr. 12–16, 2010.
4. Karttunen, A., J. Säily, A. E. I. Lamminen, J. Ala-Laurinaho, R. Sauleau, and A. V. Räisänen, "Using optimized eccentricity rexolite lens for electrical beam steering with integrated aperture coupled patch array," *Progress In Electromagnetics Research B*, Vol. 44, 345–365, 2012.
5. Artemenko, A., A. Maltsev, R. Maslennikov, A. Sevastyanov, and V. Ssorin, "Beam steerable quartz integrated lens antenna for 60 GHz frequency band," *Proc. 5th Eur. Conf. Antennas Propag.*, 788–792, Rome, Italy, Apr. 11–15, 2011.
6. Karttunen, A., J. Ala-Laurinaho, R. Sauleau, and A. V. Räisänen, "Reduction of internal reflections in low permittivity integrated lens antennas," *Proc. Millimetre Wave Days*, Espoo, Finland, May 23–25, 2011.
7. Filipovic, D. F., G. P. Gauthier, S. Raman, and G. M. Rebeiz, "Off-axis properties of silicon and quartz dielectric lens antennas,"

IEEE Trans. Antennas Propag., Vol. 45, No. 5, 760–766, May 1997.

8. Karttunen, A., J. Ala-Laurinaho, R. Sauleau, and A. V. Räisänen, "2D beam-steering with non-symmetrical beam using non-symmetrical integrated lens antenna," *Proc. 6th Eur. Conf. Antennas Propag.*, 2976–2980, Prague, Czech Republic, Mar. 25–30, 2012.
9. Van der Vorst, M. J. M., P. J. I. de Maagt, and M. H. A. J. Herben, "Scan-optimized integrated lens antennas," *Proc. 27th European Microwave Conference*, 605–610, Jerusalem, Israel, 1997.
10. Van der Vorst, M. J. M., P. J. I. de Maagt, and M. H. A. J. Herben, "Effect of internal reflections on the radiation properties and input admittance of integrated lens antennas," *IEEE Trans. Microwave Theory Tech.*, Vol. 47, No. 9, 1696–1704, Sept. 1999.
11. Van der Vorst, M. J. M., P. J. I. de Maagt, A. Neto, A. L. Ryenolds, R. M. Heeres, W. Luinge, and M. H. A. J. Herben, "Effect of internal reflections on the radiation properties and input admittance of integrated lens antennas – comparison between measurements and theory," *IEEE Trans. Microwave Theory Tech.*, Vol. 49, No. 6, 1118–1125, Jun. 2001.
12. Wu, X., G. V. Eleftheriades, and T. E. van Deventer-Perkins, "Design and characterization of single- and multiple-beam mm-wave circularly polarized substrate lens antennas for wireless communications," *IEEE Trans. Microwave Theory Tech.*, Vol. 49, No. 3, 431–441, Mar. 2001.
13. Neto, A., A. Toccafondi, and S. Maci, "Mutual coupling between slots printed at the back of elliptical dielectric lenses," *IEEE Trans. Microwave Theory Tech.*, Vol. 49, No. 6, 1118–1125, Jun. 2001.
14. Natarajan, A., S. K. Reynolds, M.-D. Tsai, S. T. Nicolson, J.-H. C. Zhan, D. G. Kam, D. Liu, Y.-L. O. Huang, A. Valdes-Garcia, and B. A. Floyd, "A fully-integrated 16-element phased-array receiver in SiGe BiCMOS for 60-GHz communications," *IEEE J. Solid-State Circuits*, Vol. 46, No. 5, 1059–1075, May 2011.
15. Ludwig, A. C., "The definition of cross polarization," *IEEE Trans. Antennas Propag.*, Vol. 21, No. 1, 116–119, Jan. 1973.